Received: 16 September 2022 | Accepted: 1 November 2022

DOI: 10.1002/hyp.14768

SPECIAL ISSUE PAPER

WILEY

# Resolving streamflow diel fluctuations in a small agricultural catchment with an integrated surface-subsurface hydrological model

Daniele la Cecilia[1,2] | Matteo Camporese[3]

[1]Department of Environmental Chemistry, Eawag, Swiss Federal Institute of Aquatic Science and Technology, Dübendorf, Switzerland

[2]Water Resources and Drinking Water, Eawag, Swiss Federal Institute of Aquatic Science and Technology, Dübendorf, Switzerland

[3]Department of Civil, Environmental and Architectural Engineering, University of Padova, Padova, Italy

**Correspondence**
Daniele la Cecilia, Department of Environmental Chemistry Eawag, Swiss Federal Institute of Aquatic Science and Technology, 8600 Dübendorf, Switzerland.
Email: daniele.lacecilia@eawag.ch

**Funding information**
Swiss Federal Office for the Environment and the Eawag Academic Transition

## Abstract

During dry periods, stream discharge in vegetated catchments can naturally fluctuate up to 10% daily. Despite intensive efforts put in observing and interpreting diel fluctuations of stream discharge across a range of instrumented natural catchments worldwide, the capability of state-of-the-art hydrological models to reproduce and explain such processes has rarely been tested. Here, we used CATHY, a physics-based integrated surface-subsurface hydrological model (ISSHM), to simulate the stream discharge in a small tile-drained agricultural catchment in Switzerland, where streamflow diel fluctuations appeared in dry periods. The model was able to satisfactorily reproduce the measured stream discharge, including the observed diel fluctuations. Next, we designed and simulated a series of modelling scenarios aimed to disentangle the processes contributing to the diel fluctuations in stream discharge. These scenarios revealed the predominant role of evapotranspiration (ET) in the establishment of diel fluctuations in stream discharge. Irrigation sustained the baseflow in dry periods and caused short-living streamflow peaks, which did not directly cause, but superposed to, diel patterns. Vegetation rooting depths and response to oxygen stress in the root zone slightly affected the amplitude of the streamflow diel fluctuations, while changes in the saturated hydraulic conductivity driven by diel soil temperature fluctuations caused an amplitude of the streamflow diel signal 10 times smaller compared to the one caused by ET. Our study demonstrates that ISSHMs such as CATHY can provide high-fidelity spatially-distributed dynamic simulations of evapotranspiration and irrigation fluxes, as well as soil moisture and groundwater flows, enhancing our understanding of the role of these hydrological processes during dry periods and thus making these models useful tools for a more sustainable management of agricultural catchments.

**KEYWORDS**
CATHY, diel fluctuations, dry conditions, headwater stream, ISSHM, low flow, tile-drains, water quantity

## 1 | INTRODUCTION

The European Alps are experiencing lusher vegetation but drier streams due to decreases in precipitation (P) and increases in evapotranspiration (ET) (Mastrotheodoros et al., 2020). As P and ET can be the largest components of the water balance (Ryken et al., 2022), the crucial role of ET in driving low flows during meteorological droughts has long been recognized (Bosch & Hewlett, 1982;

  

Czikowsky & Fitzjarrald, 2004; Haslinger et al., 2014). Indeed, during the recent summer droughts, ET contributed to the depletion of soil water storage in Europe (Teuling et al., 2013) as well as in the United States (Floriancic et al., 2021). During low-flow conditions, groundwater is typically the only supply of freshwater into the stream (Brunner et al., 2017). At the catchment scale, geology and topography contribute to drive groundwater flows, thus naturally influencing the low-flow regime of the stream (Smakhtin, 2001).

Natural streams experiencing low flows may manifest ET-driven diel streamflow fluctuations, which can further reduce by more than 10% the mean daily discharge at the sub-daily level (Lundquist & Cayan, 2002). ET is higher during the day and lower or zero at night; at the catchment scale, this signal in ET can drive diel fluctuations of stream discharge, which achieve higher values in the early morning and lower values in the late afternoon. Due to the projected increase of incoming solar longwave irradiance (Roderick et al., 2014), ET will also increase as long as soil water is available. ET may thus exacerbate the stress generated by low flows to the society and aquatic organisms (Bradford & Heinonen, 2008; Smakhtin, 2001), particularly in small streams, which have high ecological value (Biggs et al., 2016) and constitute the majority of the channel length of river networks (Wohl, 2017).

Scientists have been carrying out extensive field monitoring studies aiming to pinpoint the drivers of streamflow diel fluctuations and to study the properties of the diel signal including its source, magnitude, timing and seasonality. A mechanistic description of this phenomenon would lead to a better understanding of the connectivity of hillslope and riparian vegetation with the streams and the low-flow hydrological processes. The predominant role of vegetation as the source of diel signals was confirmed in situations where fluctuations disappeared after a fire removed all hillslope, riparian and in-stream vegetation (Lawrence, 1990; O'Laughlin et al., 1982). Other processes could only partly explained diel fluctuations and they included fluctuations in atmospheric pressure (Turk, 1975), temperature-induced variability in the viscosity of stream water leading to greater streambed losses (Constantz, 1998), and thermal expansion of water (Czikowsky & Fitzjarrald, 2004).

The role of vegetation on the establishment of diel streamflow fluctuations was conceptualized with two main basic hypotheses in the last 30 years (depicted in figure 3 in Harmon et al. (2020) or in figure 5 in Kirchner et al. (2020). Burt (1979) hypothesized that during the day evapotranspiration drives an upward flux of soil moisture, which shrinks the saturated wedge that contributes to lateral subsurface flow from hillslopes to the stream. At night, ET ceases and the lateral subsurface flow from the saturated wedge can increase. Bren (1997) concluded that riparian vegetation predominantly intercepted water from saturated and unsaturated lateral subsurface flow paths draining hillslope storage, resulting in a diel signal expressed at the stream channel. In addition to these two main mechanisms, Bond et al. (2002) proposed a flow path migration hypothesis that can disconnect hillslope and riparian vegetation from the stream channel when the groundwater table drops. As the subsurface lateral flow shifts towards deeper, slower flow paths, both in the hyporheic zone and from the hillslopes, signal propagation to the stream becomes slower. However, a great number of field studies worldwide depict situations where these hypotheses are not mutually exclusive but rather coexist on a continuum of hillslope–riparian hydrological processes (Harmon et al., 2020).

Szeles et al. (2018) showed that studies aiming to underpin the causal link between the complex process drivers and the streamflow signal at the daily and seasonal scales would require the collection of data adequately resolved in space and time for all the relevant hydrological and terrestrial compartments. These data, such as streamflow at the catchment outlet as well as groundwater depth and evapotranspiration over the catchment, can be modelled by means of state-of-the-art integrated surface-subsurface hydrological models (ISSHMs) (Paniconi & Putti, 2015). However, to the best of our knowledge, ISSHMs have not been used yet to reproduce and investigate observed diel streamflow fluctuations.

In this study, we applied the physics-based CATchment HYdrology (CATHY) model to reproduce the diel streamflow fluctuations during low-flow periods observed during a short-term field investigation in a small tile-drained agricultural catchment. Due to the complex topography, heterogeneous vegetation types and varying hydrometeorological boundary conditions, there was uncertainty on the sources of the observed diel signals. Thus, the overarching goals of the study were to (1) understand the influence of human interventions (i.e., irrigation) on the occurrence of diel streamflow fluctuations, (2) explore the consequences of different parametrizations of vegetation properties (i.e., response to oxygen stress and different rooting depths) on the hydrological budget over the catchment and (3) quantify the changes in diel streamflow signal properties with a suite of hypothetical scenarios.

## 2 | METHODS

### 2.1 | Study area

We studied a small tile-drained agricultural catchment (2.67 $km^2$) in the Swiss Plateau close to Lake Constance (Figure 1). The catchment was chosen in the context of an innovative high-frequency water quality monitoring campaign (la Cecilia, Dax, Ehmann, et al., 2021), conducted between May 27th and July 7th 2019, which resulted in the collection of hydrological data leading to the observation of diel fluctuations in stream discharge. The catchment is hilly, with a median slope of about 3%, as calculated from the digital terrain model (DTM) swissALT3D2019, which represents the surface of Switzerland without vegetation and development, available at 0.5 m pixel resolution at the website https://geovite.ethz.ch/DigitalElevationModels.html. The same DTM has been used to generate the computational mesh of the catchment, as described in Section 2.4.

### 2.2 | Land use

Land use is mainly agricultural, with urbanization below 1%. Forests are present in the upper part of the catchment and riparian trees are

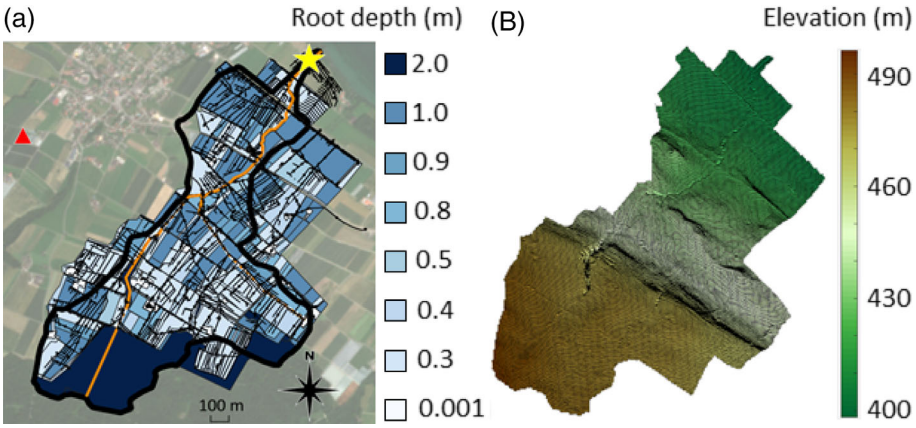


**FIGURE 1** Study area. (a) Root depth map specified at parcel level as colour filled areas, weather station as red triangle, main stream network in orange line, tile drain network as black lines, gauging station at the catchment outlet in 2019 coinciding with the yellow star, topographic catchment as black thick line. Background is the true colour image from Sentinel-2 at 10 m pixel resolution sensed on June 26th, 2019. (b) Digital terrain model of the studied catchment at 10 m resolution (source: swissALT3D2019)

found all along the open stream. The agricultural land use in the catchment for 2019 was compiled by the Cantonal Authority of Thurgau and defined agricultural lands at the parcel level (Landwirtschaftliche Bewirtschaftung; available at https://www.geodienste.ch/downloads/lwb_nutzungsflaechen) (Table S1). The overall 41 agricultural land uses were aggregated in eight major classes based on their similarity in rooting depth, which is an important information layer for the chosen hydrological model CATHY (Table 1). To these classes we assigned the root depth based on FAO guidelines (Allen et al., 2006) when available; we used reasonable values otherwise (Table S1). The root distribution density was assumed to linearly decrease along its depth.

## 2.3 | Hydrometeorological data

Weather data and soil temperature at 5, 10 and 20 cm depth with 1-h resolution were obtained from a gauging station (Güttingen—GUT) maintained by the Swiss Federal Office of Meteorology and Climatology (MeteoSwiss). The station is located at 47°36′ N and 9° 17′ E, at a distance of 1.8 km from the catchment outlet. Given the small extension of the catchment, we assumed the weather data to be homogeneous in space. The weather data included rainfall (P) and all the variables needed to calculate the potential evapotranspiration (ET), such as mean air temperature measured at 2 m from the ground, air relative humidity, mean wind speed at 2 m height, and global solar radiation. Hourly ET ($ET_{hour}$) was calculated following the approach suggested by FAO for hourly input data (Allen et al., 2006) (light green line in Figure S1a). Negative values, which might occur when working at the hourly time scale, were forced to 0. The calculated daily sum of $ET_{hour}$ ($ET_{day}$) (dark green line in Figure S1b) was compared with the daily ET provided by MeteoSwiss ($ET_{MS,day}$) for the same station (grey line in Figure S1b), which was calculated based on the approach suggested by FAO for daily input data (Allen et al., 2006). As $ET_{day}$ was lower than $ET_{MS,day}$ by a day-specific factor ranging from 1.3 to 2.6, we scaled up $ET_{hour}$ to calculate $ET_{hour,scaled}$ (black line in Figure S1a) as:

$$ET_{hour,scaled} = \frac{ET_{MS,day}}{ET_{day}} \times ET_{hour}, \quad (1)$$

**TABLE 1** Aggregated land uses, the corresponding cumulative areas in hectares, the prescribed root depths based on FAO guidelines (Allen et al., 2006)

| Aggregated land uses | Area (ha) | Aggregated land use with root depth of (m) |
|---|---|---|
| Urban areas and roads | 5.3 | 0.001 |
| Annual floriculture, flower strips for pollinators and other useful organisms, Artificial meadows (without pasture), extensive meadows (without pasture), Little intensive meadows (without pasture), other perennial meadows (without pasture), pasture, extensive pasture, other vegetated areas, Floriculture in greenhouses, bushes and strips, other agricultural areas (with contributions), other agricultural areas (without contributions), Walking paths | 84.6 | 0.3 |
| Potatoes | 1.3 | 0.4 |
| Annual vegetables, strawberries, Asparagus, vegetables in greenhouses, other specialty crops in greenhouses | 18.5 | 0.4 |
| Sugarbeets and beet roots | 8.5 | 0.5 |
| Perennial berries and other nurseries (orchards) | 15.2 | 0.8 |
| Corn and corn for silage | 15.3 | 0.9 |
| Winter barley, Wheat (Swiss granum), Winter wheat, Winter canola, Apples, Pears, Orchards, Christmas trees, Bushes and shrubs, Other orchards (kiwi, etc…) | 73.7 | 1 |
| Forests, other forests, riparian vegetation | 45.3 | 2 |

*Note*: Land uses from the detailed classification retrieved from the Swiss Federal Office of Topography (SwissTopo) are provided in Table S1.

which allowed us to prescribe an overall realistic meteorological forcing with a signal frequency necessary for modelling the process of diel fluctuations. We homogeneously applied $ET_{hour,scaled}$ in the catchment excluding the urban areas.

Water level in the stream was gauged at the outlet, an artificial rectangular cross section, by the environmental office of the Canton Thurgau every 15 min. As no rating curve was available, we approximated the discharge ($Q_{observed}$ in $m^3\ s^{-1}$) using the Gauckler–Strickler formula:

$$Q_{observed} = GS \times R_H^{2/3} \times i_f^{1/2} \times A, \quad (2)$$

where *GS* is the Gauckler–Strickler coefficient, here assumed equal to 18 $m^{1/3}\ s^{-1}$, $R_H$ is the hydraulic radius, $i_f$ is the slope of the stream, calculated using the altitude reported in the digital elevation model at the outlet and a second location 131.3 m upstream (i.e., $i_f$ = [401.7–397.8 m] / 131.3 m), and *A* is the area of the stream given the width of the rectangular section, that is, 1.54 m.

## 2.4 | CATchment HYdrology model (CATHY)

The CATchment HYdrology (CATHY) model is a physics-based ISSHM, which accounts for the interactions among surface water, groundwater and vegetation. The subsurface module solves the 3D Richardson-Richards equation for variably saturated porous media with a finite element method and the surface module solves the diffusion wave approximation of the shallow water equation with an explicit finite difference scheme (Camporese et al., 2010).

The CATHY model uses the Feddes approach (Camporese et al., 2015) to calculate the water stress function $\propto$ as a function of the pressure head ψ, which computes the actual ET based on the vegetation response as $ET_{hour,scaled} \times \propto(\psi)$, where:

$$\propto(\psi) = \begin{cases} 0 \ \text{when} \ \psi < \psi_{wp} \\ \dfrac{\psi - \psi_{wp}}{\psi_d - \psi_{wp}} \ \text{when} \ \psi_{wp} < \psi < \psi_d \\ 1 \ \text{when} \ \psi_d < \psi < \psi_{an} \\ 1 - \dfrac{\psi - \psi_{an}}{\psi_s - \psi_{an}} \ \text{when} \ \psi_{an} < \psi < \psi_s \\ 0 \ \text{when} \ \psi > \psi_s \end{cases}, \quad (3)$$

where $\psi_{wp}$ is the pressure head at the wilting point, $\psi_d$ is the pressure head that starts causing stress to the vegetation, $\psi_{an}$ is the anaerobiosis limit beyond which the plant starts to suffer excess soil water and $\psi_s$ is the pressure head at saturation.

### 2.4.1 | Model set-up and reference simulation

The numerical grid was built on the basis of a down-sampled 20 m-resolution DTM of the study area. This spatial resolution was a trade-off between the necessary level of details to simulate the catchment with hourly boundary conditions over 48 days and the time needed to run one full simulation, which typically lasts about 2–3 h on an openstack-based cloud virtual machine (http://cloudveneto.it/). The resulting numerical grid, with a vertical discretization as reported below, has a total of 79 849 nodes and 418 140 tetrahedral elements.

The soil in the catchment is predominantly silty and overlays moraine deposits (Source: Swiss Federal Office of Topography—Weinfelden, LK 1054—available at https://shop.swisstopo.admin.ch/en/maps/geological-maps/geological-atlas-switzerland-25000). Based on stratigraphic information, we modelled a total soil thickness of 5 m, assuming an impermeable layer as the bottom boundary condition. The soil thickness was discretised into 10 numerical layers parallel to the ground surface, their thickness gradually increasing with depth, from 5 cm at the surface to 1 m at the bottom. The soil type suggested relatively low hydraulic conductivity values and we assumed average soil parameter values from (Carsel & Parrish, 1988) as first guess (Table 2). We used the Van Genuchten (1980) model to calculate the volumetric soil water content and unsaturated hydraulic conductivity as a function of the matric potential (parameter values reported in Table 2). All soil hydraulic properties were assumed spatially uniform, given the lack of spatially explicit information about soil parameters.

We then ran a sensitivity analysis on the saturated hydraulic conductivity (Ks) considering a range of values between $1.88 \times 10^{-5}$ and $1.88 \times 10^{-3}$ m $s^{-1}$ (Table S2) to estimate the homogeneous equivalent value that best reproduce the streamflow dynamics. We found this value to be Ks = $1.0 \times 10^{-4}$ m $s^{-1}$ (Figure S2).

In the final step of the model refinement, that is, the reference simulation, we represented the widespread presence of tile drains in the catchment (black lines in Figure 1; Source: Planimpuls.ch) by an equivalent more conductive porous medium layer, similarly to Rozemeijer et al., (2010). In doing so, we increased the Ks of the numerical layer at a depth where tile drains are expected (1 m depth) and 60 cm thick to account for soil disturbances and the typical presence of highly permeable filling material above and below the drains (i.e., the numerical layer between 80 and 140 cm depth). We increased the Ks of this 'tile drain'

**TABLE 2** Soil properties and hydraulic parameters for the reference simulation

| Depth (cm) | Porosity (–) | Residual moisture content (–) | Van Genuchten $\propto$ ($cm^{-1}$) | Van Genuchten n (–) | Specific storage coefficient ($m^{-1}$) | Saturated hydraulic conductivity ($ms^{-1}$) |
|---|---|---|---|---|---|---|
| 0–80 | 0.43 | 0.078 | 0.036 | 1.56 | $1.00 \times 10^{-3}$ | $7.3 \times 10^{-5}$ |
| 80–140 (Tile-drain) | 0.43 | 0.078 | 0.036 | 1.56 | $1.00 \times 10^{-3}$ | $1.0 \times 10^{-3}$ |
| 140–500 | 0.43 | 0.078 | 0.036 | 1.56 | $1.00 \times 10^{-3}$ | $7.3 \times 10^{-5}$ |

layer and we reduced the Ks of the other layers by constraining the geometric mean of Ks to be equal to the previous equivalent homogeneous Ks (i.e., Ks = $1.0 \times 10^{-4}$ m $s^{-1}$). We chose the geometric mean because it is more appropriate than the arithmetic or harmonic means when the groundwater flow is sometimes parallel to the ground profile (i.e., during recession) and sometimes vertical (e.g., during infiltration). The resulting Ks for the 'tile drain' layer was $1.0 \times 10^{-3}$ m $s^{-1}$ and the Ks for the other layers was $7.3 \times 10^{-5}$ m $s^{-1}$. The network of tile drains connected to the stream an estimated additional surface of 0.67 $km^2$, which was included in our numerical domain.

The simulations were initialised with a warm-up period from 11th April to 26th May, with initial conditions consisting in a spatially uniform water table at 0.5 m depth. Based on a preliminary sensitivity analysis, whereby we also started with a fully saturated catchment and a water table depth of 1.0 m, the warm-up period was sufficient to obtain results basically unaffected by the initial conditions. The period of interest, used to compute the goodness of fit, goes from the 26th of May to the 7th of July 2019. The goodness of fit between the streamflow estimated from water level measurements and the one simulated by CATHY was calculated by means of four generally accepted evaluation metrics. These were the Kling-Gupta Efficiency index (KGE) (Gupta et al., 2009), Nash-Sutcliffe Efficiency index (NSE) (Nash & Sutcliffe, 1970), Willmott index of agreement (WioA) (Willmott, 1984) and root mean square error (RMSE).

No flux boundary conditions were imposed at the bottom and lateral boundaries of the computational domain, whereas net precipitation, that is, rainfall minus $ET_{hour,scaled}$, was used as atmospheric forcing on forests and riparian trees, net precipitation plus irrigation (at 90% field application efficiency) on agricultural areas and rainfall on urban areas. Irrigation was applied in the catchment given the presence of high-value crops and vegetables served with drip lines, but the schedule and quantity were not known. To investigate the role of irrigation on streamflow, we estimated the daily irrigation as equal to the maximum between 0 mm/day and the difference between daily rainfall and ET (i.e., $ET_{MS,day}$). Then, we homogeneously applied only on agricultural lands the estimated daily irrigation, reduced to 90% to account for potential losses, equally distributed in two events scheduled between 7 am–8 am and between 5 pm–6 pm.

In CATHY, Gauckler–Strickler coefficients for surface flow vary dynamically with discharge according to scaling properties of stream geometry, that is, 'at-a-station' and 'downstream' relationships (Camporese et al., 2010). In all the simulations, we assumed a Gauckler–Strickler coefficient of 10 $m^{1/3}$ $s^{-1}$ for the stream channel and of 1 $m^{1/3}$ $s^{-1}$ for the hillslope, relative to a reference catchment area of 2.7 $km^2$ and a reference discharge of 0.1 $m^3$ $s^{-1}$.

## 2.5 | Hypothetical simulation scenarios

Given the capability of catchment-scale process-based models to be used for hypothesis testing, we designed and tested, starting from the reference simulation described in the previous section, four hypothetical scenarios aimed at assessing the influence of relevant model parameters and process representations on streamflow diel fluctuations.

We started with Scenario 1, by excluding irrigation from the reference simulation. This scenario serves primarily to assess the differences between an agricultural catchment and a natural one. Note that here we do not explicitly model agricultural practices such as tilling, ploughing, harvesting, etc. However, given the relatively short modelled period we can safely assume that land management operations did not have a strong impact on the modelled scenarios.

In Scenario 2, we additionally excluded the effect of oxygen stress, whereby roots could take up water even when soil moisture exceeded a threshold according to the Feddes approach (Equation (3)).

We considered two test cases in Scenario 3. Starting from Scenario 2, we assumed a homogeneous rooting depth of 0.3 m in the first case and of 2.0 m in the second one. This allowed us to assess the influences of the capability of vegetation to access only shallow or also deep soil water and the consequences in driving different patterns of groundwater levels and subsurface water flow.

In Scenario 4, we investigated the effect of saturated hydraulic conductivity varying with soil temperature, as the dynamic viscosity of water changes as a function of temperature and, as a result, the hydraulic conductivity might follow daily temperature patterns and drive diel fluctuations in soil water content and stream discharge (Schwab et al., 2016). Time-variable Ks for this scenario (Figure S3) was calculated using the procedure described as follows.

The air temperature measured by MeteoSwiss during the study period was used as the top boundary condition for a 1D model of heat transport within a homogeneous medium having the same soil thickness of the modelled domain. Using a bulk thermal diffusivity of $1.43 \times 10^{-7}$ $m^2$ $s^{-1}$, we computed the time series of soil temperature in the same numerical layers as in the CATHY model. Compared to the soil temperature measured by MeteoSwiss at 5, 10 and 20 cm depth, the computed soil temperature exhibit slightly overestimated fluctuations.

The modelled temperature, T, in degrees Kelvin (K) was used to calculate the dynamic viscosity, μ (Pa s), as in (Gutmann & Simmons, 1952):

$$\mu = A \times 10^{\frac{B}{T-C}} \tag{4}$$

where $A = 2.414 \times 10^{-5}$ Pa s, $B = 247.8$ K, and $C = 140$ K (at 20°C, $\mu = 1.001 \times 10^{-3}$ Pa).

The soil temperature-dependent hydraulic conductivity was then calculated as:

$$\mathrm{Ks}(\mathrm{T}) = \frac{k \times g \times \rho}{\mu(T)} \tag{5}$$

where $k$ is the intrinsic permeability corresponding to the reference values of $K_s = 1.0 \times 10^{-3}$ m $s^{-1}$ for the 'tile-drain' layer and of Ks = $7.3 \times 10^{-5}$ m $s^{-1}$ for the other layers (i.e., $k = 1.023 \times 10^{-11}$ and $k = 7.468 \times 10^{-12}$, respectively), $g = 9.81$ m $s^{-2}$ is the gravity acceleration, and $\rho = 998.2071$ kg $m^{-3}$ is the density of water at the reference temperature of 20 °C. To better highlight the possible diel fluctuations resulting in this scenario, we excluded ET from the

atmospheric forcing, to prevent its periodic signal in the modelled system from masking the soil temperature-induced fluctuations.

### 2.6 | Post-processing of relevant outputs

We compared the streamflow time series simulated in the different scenarios in order to visualize what hypotheses better explained the occurrence of diel streamflow fluctuations. In addition, we detrended the time series of simulated streamflow at the outlet and of groundwater depth (GWD) for all grid nodes so as to filter out the progressive decrease typical of draining/recession phases in dry periods. The detrending consisted in subtracting the best-fit line, obtained with the linear least-squares method, from the time series (procedure exemplified in Figure S4). This allowed for better analysing the diel fluctuations of streamflow and GWD in dry periods. The detrended time series were annotated with the subscript $_{dt}$.

CATHY saved the time series of actual ET and GWD for all grid node of the computational domain in the selected dry period. As a first step, we calculated and mapped the mean of daily maximum actual ET and mean GWD to describe general differences in hydrological quantities among the hypothetical scenarios. Next, for each scenario, we used $GWD_{dt}$ time series for all grid nodes relative to the dry period to calculate the amplitude of diel fluctuations as the absolute difference between the maximum and the minimum $GWD_{dt}$ values for each dry day.

Finally, we carried out a target analysis using $GWD_{dt}$ time series of Scenario 1 to identify general patterns related to the timing of GWD diel fluctuations. Scenario 1 was the hypothetical simulation without irrigation and it was chosen so as to conceptualize a 'natural' vegetated catchment. We clustered the grid nodes where GWD followed similar dynamics over the selected dry period. Thus, we created 5 clusters and we populated them with $GWD_{dt}$ time series of the grid nodes which had mean GWD within the same range of depth ($\overline{GWD_z}$) (with the range of depth spanning from 0 m to 5 m by 1 m and with $z$ varying from 1 to 5 to identify the 5 clusters). We calculated for each grid node the daily absolute difference between maximum and minimum $GWD_{dt}$ (i.e., the amplitude called here $|\Delta GWD_{dt}|$) and we determined after how many days $|\Delta GWD|$ was achieved following the beginning of the dry period. Then, within each cluster $z$, we averaged the $GWD_{dt}$ of those grid nodes having the same number of days to achieve the largest $|\Delta GWD_{dt,z}|$ over the dry period.

## 3 | RESULTS

In this section, we first present the calibrated reference simulation to demonstrate the capability of CATHY to realistically replicate the observed discharge, including the diel fluctuations. Then, we present the modelling hypothetical scenarios with changing vegetation and soil properties to describe and disentangle the hydrological processes controlling streamflow diel fluctuations in a tile-drained agricultural catchment. Finally, we show target analyses on the Scenario 1 simulation (i.e., without irrigation) to expand the insights on the link between spatial and temporal features of hydrological processes at the catchment scale and the streamflow at the outlet gained by means of CATHY.

### 3.1 | Reference simulation

As described in Section 2.4.1, the calibrated model representing the reference simulation had a Ks of the 'tile drain' layer equal to $1.0 \times 10^{-3}$ m s$^{-1}$ and a Ks of the other layers equal to $7.3 \times 10^{-5}$ m s$^{-1}$; it accounted for oxygen stress in the Feddes formula (i.e., $\psi_{an} \cong \psi_s = 0\,m$, with $\psi_{wp} = -150$ m and $\psi_d = -4$ m), with heterogeneous rooting depths between 0.3 m to 2 m, used all hydrological forcings as boundary conditions (i.e., rainfall, ET and irrigation), and was initialised with the groundwater table at 0.5 m depth. With these settings, CATHY predicted reasonably well the stream discharge with a KGE of 0.68, NSE of 0.68, WioA of 0.88 and RMSE of 0.04 m$^3$ s$^{-1}$. More importantly, the model was able to replicate the process of stream discharge diel fluctuations, observed in the two dry periods: the first from June 2nd to June 8th and the second from June 22nd to June 30th (the latter depicted in Figure 2b). In these periods, peak discharges at the outlet occurred at night and lagged the peaks in ET that occurred during the day. Notably, the assumption of applying irrigation in the early morning and late afternoon matched the dynamics of some of the measured short-living streamflow peaks, as evident in Figure 2b, even though those are overestimated by the model. While an accurate description of irrigation practices was not the scope of this research, improvement in the model output could be achieved by fine-tuning irrigation timing and amount given that agricultural lands were certainly not all irrigated at the same time.

### 3.2 | Hypothetical scenarios and the implications on streamflow

We tested four hypothetical scenarios as described in Section 2.5 to understand the potential role of different parameters and processes on the occurrence of diel streamflow fluctuations.

We began by removing irrigation in Scenario 1. The results indicated that the streamflow significantly decreased without irrigation (Figure 3a) but diel fluctuations in the detrended streamflow still occurred in the dry period (Figure 3b). As expected, the short-living streamflow peaks in the early morning and in the late afternoon disappeared without irrigation (Figure 3b). Our simulations showed that irrigation led to substantial differences in catchment hydrology during dry periods, but it did not alter the typical pattern of diel streamflow fluctuations in this catchment.

In Scenario 2, we simulated how catchment hydrology changes when vegetation was influenced by oxygen stress ($\psi_{an} \cong \psi_s = 0$ m) or not ($\psi_{an} > 5$ m). The streamflow was lower when vegetation was not influenced by oxygen stress according to the Feddes model (Figure 3c), due to the capability of vegetation to take up water also in

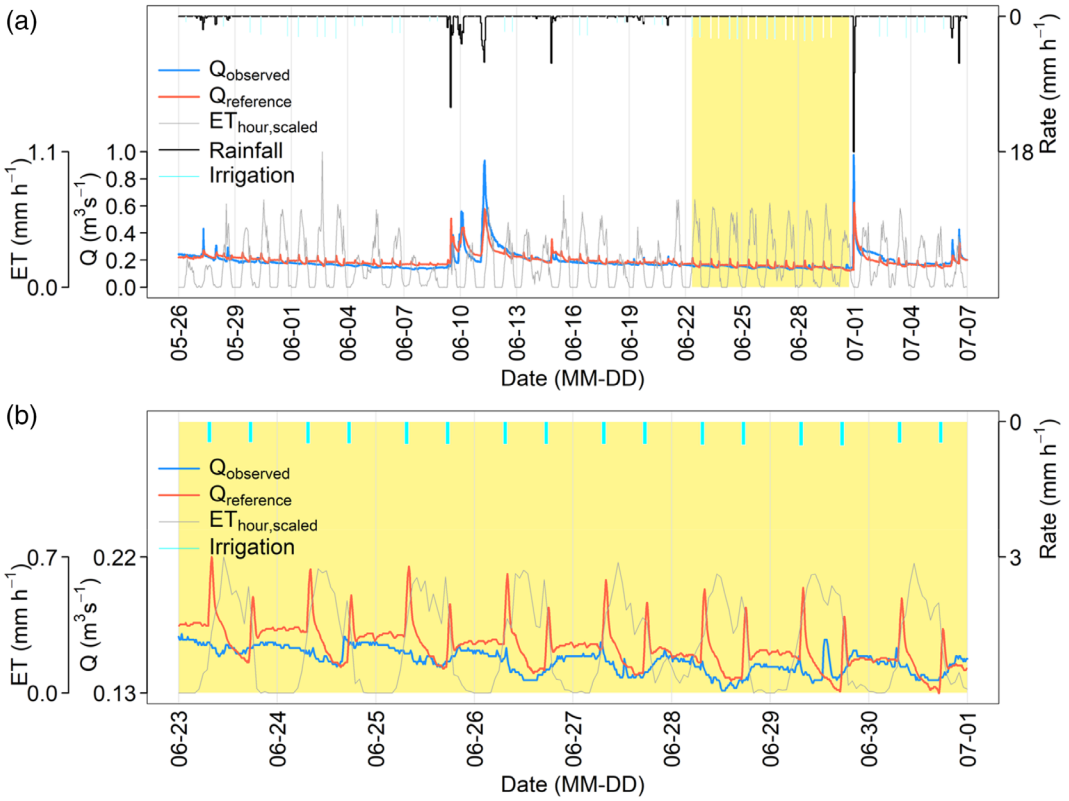


**FIGURE 2** (a) Time series of observed ($Q_{observed}$) and simulated ($Q_{reference}$) discharge in the reference simulation, $ET_{hour,scaled}$, assumed irrigation and observed rainfall in the reversed *y*-axis. (b) Same variables as in panel a) zoomed in on the second dry period spanning from 23rd June to 30th June.

saturated areas, which increased ET (Figure S5). The amplitude of the diel fluctuations of detrended streamflow was exacerbated without oxygen stress, with an even lower minimum during the day but a larger maximum during the night as compared to the simulation with oxygen stress (Figure 3d).

In Scenario 3, disregarding the inhibitory role of oxygen stress on ET as in Scenario 2, we considered two simulations with two different homogeneous rooting depths, 0.3 m and 2.0 m (the two ends of the rooting depth range in the reference simulation). In this scenario, the streamflow modelled using the lowest rooting depth was higher than the streamflow simulated using the highest rooting depth (Figure 3e), due to increased capability of the vegetation in the latter to access deeper soil water, which increased ET (Figure S5). The modelled streamflow of Scenario 2 (heterogeneous rooting depth) was in between the two new simulated time series of streamflow. In general, the amplitude of the diel fluctuations of detrended streamflow were the largest with the highest rooting depth and the smallest with the lowest rooting depth (Figure 3f), even though in this catchment the effect of changing rooting depth is marginal.

In the last hypothesis-testing scenario, we considered Scenario 2 with no irrigation and no oxygen stress, but assumed time-variable water viscosity for the heterogeneous soil profile following temperature fluctuations and using rainfall as the only meteorological forcing, to rule out the diel patterns generated by ET. Without ET, the streamflow almost doubled as compared to the observed streamflow (or the reference simulation) and showed a very slow recession phase during the dry period, which was not in agreement with the measured recession curves (Figure 3g). However, the most important finding in this scenario is that visible diel streamflow fluctuations disappeared. We quantified the negligible influence of varying hydraulic conductivity on the occurrence of diel streamflow fluctuations after detrending the streamflow time series. While the mean amplitude of observed streamflow fluctuations was 0.02 $m^3\ s^{-1}$ during the dry period, with an average streamflow of about 0.2 $m^3\ s^{-1}$ (Figure 3h), in Scenario 4, the mean daily amplitude was in the order of 0.002 $m^3\ s^{-1}$, about 10 times smaller than observed, despite a higher predicted streamflow of 0.4 $m^3\ s^{-1}$. Also, the streamflow fluctuations were out-of-phase with the observed patterns, thus corroborating that this process could not explain our measurements and confirming the fundamental role of ET for the establishment of diel streamflow fluctuations.

## 3.3 | Hypothetical scenarios and the implications on ET and groundwater depth

Over the 8-day dry period from 23rd June to 30th June , the average values of daily maximum actual ET fluxes ranged between 0 and 0.48 mm $h^{-1}$ across all simulations (left panels of Figure 4) and the

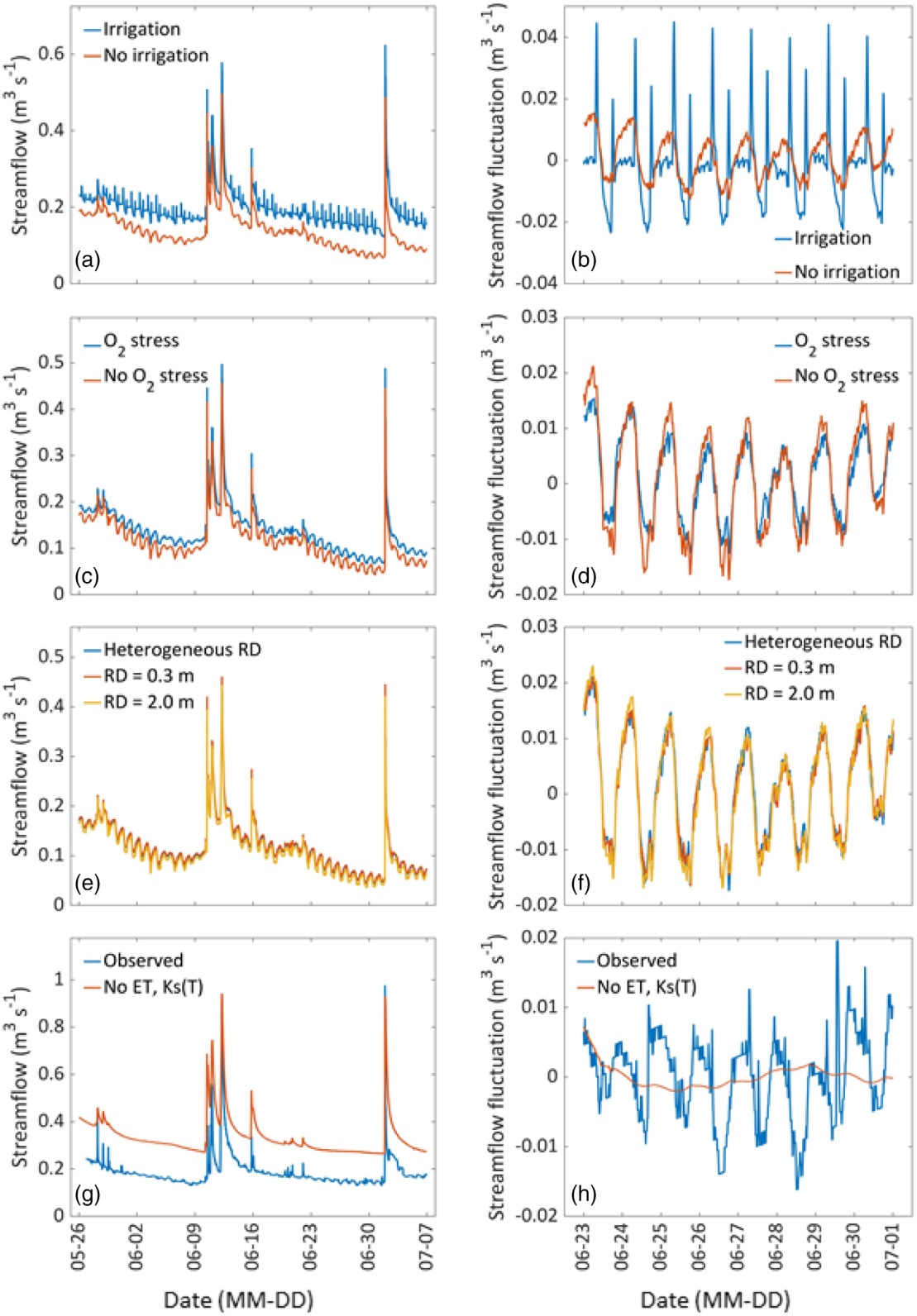


**FIGURE 3** Time series of the streamflow (simulated or observed) in the whole period of interest (panels on the left) and detrended streamflow time series in the second dry period from June 23rd to 30th (panels on the right). (a) and (b) Reference simulation and Scenario 1 (without irrigation). (c) and (d) Scenario 1 (with oxygen stress) and Scenario 2 (without oxygen stress). (e) and (f) Scenario 2 for heterogeneous rooting depth (RD) and Scenario 3 for homogeneous RD at 0.3 m and 2.0 m. (g) and (h) Observed streamflow and Scenario 4 (Ks as a function of temperature T and without ET).

average values of GWD spanned over the whole soil profile between 0 and 5 m (right panels in Figure 4). However, depending on the scenario, we obtained largely different spatial patterns of actual ET and, to a lesser extent, GWD. The scenarios including the inhibitory effect of excess soil moisture on ET highlighted a low actual ET along the stream network (Figure 4a, c) where GWD was at 0 m (Figure 4b, d); actual ET substantially increased in the riparian zones immediately adjacent to the stream network as GWD increased. By contrast, the reference simulation (with irrigation) resulted in a shallower groundwater table as compared to Scenario 1 (without irrigation) (Figure 4b compared to Figure 4d). This, depending on the combination of topography and rooting depth, reduced ET in the downstream part of the

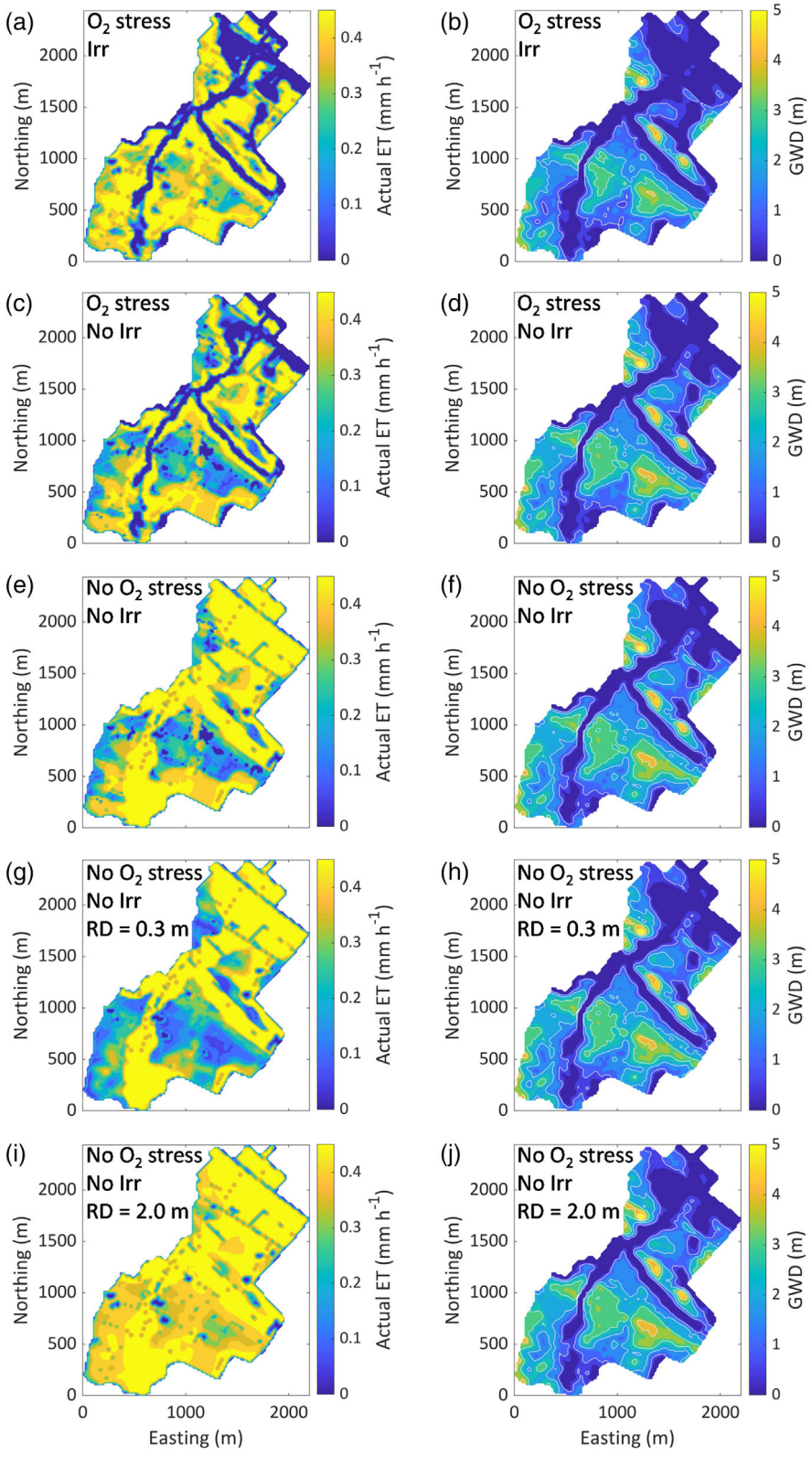


**FIGURE 4** Analyses of the second dry period from 23rd of June to 30th of June. Maps of the mean of daily maximum actual ET fluxes calculated by CATHY with the Feddes model in panel (a) for the reference simulation, (c) for Scenario 1, (e) for Scenario 2, (g) for scenario 3 with homogeneous rooting depth (RD) of 0.3 m and (i) for Scenario 3 with homogeneous rooting depth (RD) of 2.0 m. Maps of mean groundwater depth (GWD) with contour lines in white (from 1 to 5 m at 1 m intervals) in panel (b) for the reference simulation, (d) for Scenario 1, (f) for Scenario 2, (h) for Scenario 3 with homogeneous rooting depth (RD) of 0.3 m and (j) for Scenario 3 with homogeneous rooting depth (RD) of 2.0 m

catchment but increased ET in the upstream part (Figure 4a against Figure 4c). Neglecting oxygen stress resulted in a widespread increase in actual ET, also in the riparian zones where the groundwater table was shallow, as long as vegetation could reach soil water with its roots (Figure 4e–j). In fact, the comparison between the scenarios hypothesising short and long rooting depth revealed areas in the catchment where ET was limited exclusively by the depth of the groundwater table in relation with the rooting depth.

In order to investigate in more detail the sources of the diel streamflow fluctuations, we calculated the maximum diel $GWD_{dt}$ fluctuations (using detrended time series) for each grid node over the dry period for all scenarios. In Figure 5a, we showed the map relative to

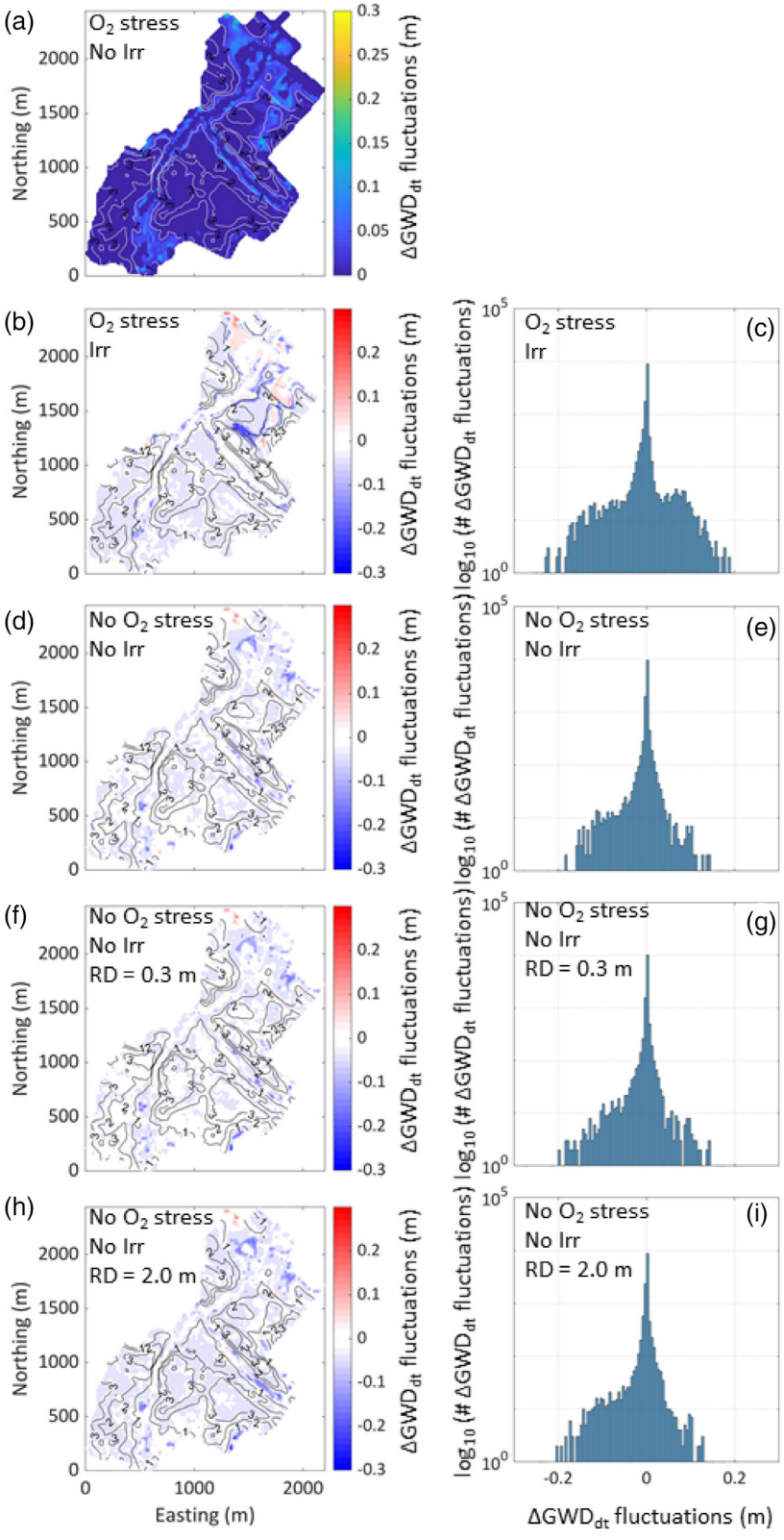


**FIGURE 5** Analyses of the second dry period from 23rd of June to 30th of June. (a) Maximum diel fluctuations of detrended groundwater depths ($\Delta GWD_{dt}$) per grid node in Scenario 1. (b) Difference between panel (a) and the same variable relative to the reference scenarios. (c) Histogram of the values in panel (b). (d) Difference between panel (a) and the same variable relative to Scenario 2. e) Histogram of the values in panel (c). (f) Difference between panel (a) and the same variable relative to Scenario 3 with homogeneous rooting depth (RD) of 0.3 m. (g) Histogram of the values in panel (f). (h) Difference between panel (a) and the same variable relative to Scenario 3 with homogeneous rooting depth (RD) of 2.0 m. (i) Histogram of the values in panel (h). White contour lines in panels (a), (b), (d), (f) and (h) depicted the mean GWD at 1, 2 and 3 m calculated for Scenario 1. The y-axis of the histograms were $\log_{10}$ scaled and had a bin width of 0.005

the 'natural' (without irrigation) Scenario 1, where $GWD_{dt}$ fluctuations ranged from 0 m to about 0.2 m. It can be clearly seen that in the nodes along the stream network, which remain always saturated, $GWD_{dt}$ diel fluctuations were negligible. Moving away from the saturated areas, the main $GWD_{dt}$ diel fluctuations occurred in relatively limited portions of the catchment, in close proximity of the riparian zones, and then decreased as the water table grew deeper than the rooting depth and actual ET declined.

The implications of the different scenarios on the diel $GWD_{dt}$ fluctuations can be clearly seen upon calculating the difference between Figure 5a and the same variable corresponding to each scenario. Irrigation caused unexpected patterns due to the nonlinearities generated by the interplay among ET with the Feddes model, GWD, rooting depth and topography. For example, fluctuations decreased (positive differences) downstream (Figure 5b) where the groundwater table was shallow (as was shown in Figure 4b), while they increased (negative differences) upstream where the groundwater table rose from below 2 m depth to above 2 m depth. We also noticed that the amplitude of the fluctuations did not change in most of the grid nodes and that on average the number of grid nodes with positive and negative differences was about the same (histogram in Figure 5c with the *y*-axis in $\log_{10}$). Consistent with previous analyses, removing the oxygen stress resulted in a widespread increase in diel fluctuations (negative differences) (Figure 5d, e). For the scenario with homogeneous shallow (0.3 m) rooting depth (Figure 5f, g) the area with larger diel fluctuations than in Figure 5a slightly contracted with respect to the scenario with heterogeneous rooting depths (Figure 5d). The opposite happened in the scenario with homogeneous deep (2.0 m) rooting depth, where the area of larger diel fluctuations expanded (Figure 5h, i).

## 3.4 | Analyses on the timing of diel fluctuations in the catchment

In the previous section, we studied spatial patterns related to diel $GWD_{dt}$ fluctuations. We followed the procedure outlined in Section 2.6 to investigate the timing of the diel fluctuations during the second dry period. Here, we used Scenario 1 to conceptualize a 'natural' (no irrigation) catchment. The average $GWD_{dt}$ time series by cluster of grid nodes with similar $\overline{GWD_z}$ revealed that diel $GWD_{dt}$ fluctuations occurred mainly where the groundwater depth was within the shallowest 2 m of soil (Figure 6a), which, not surprisingly, corresponded to the maximum rooting depth. On average, $GWD_{dt}$ achieved diel fluctuations of 2 cm in the first meter ($z = 1$) and of 0.5 cm in the second meter ($z = 2$). The calculated average behaviour encompassed the dynamics of many grid nodes spread over the catchment. Therefore, one could expect differences in the on-setting of diel fluctuations among the grid nodes. For example, considering the cluster $GWD_1$, in some grid nodes the maximum fluctuation originated early and smoothed out over time ('days to max $\Delta|GWD_{dt,1}|$' equal to 1 in Figure 6b), whereas for others the maximum amplitude of the fluctuation was achieved at a later stage ('days to max $\Delta|GWD_{dt,1}|$' equal to 8 in Figure 6b). This analysis showed that different part of catchments showed diel patterns at different point in time. Similar conclusions were reached for cluster $GWD_2$ (depicted in Figure 6c).

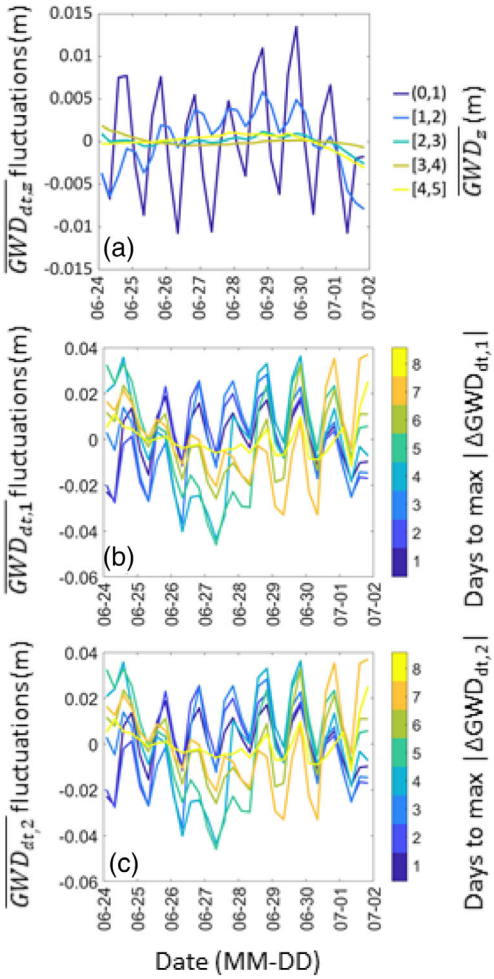


**FIGURE 6** Analyses of the second dry period from 23rd of June to 30th of June. (a) Mean detrended groundwater depths ($\overline{GWD_{dt,z}}$ fluctuations) over time calculated for grid nodes having a mean GWD within the same range of depths ($\overline{GWD_z}$) (with *z* ranging from 0 to 5 m with 1 m intervals). (b) For $\overline{GWD_1}$, we calculated the daily difference in detrended groundwater depth per grid node (i.e., $|\Delta GWD_{dt,1}|$) and the corresponding number of days when the maximum $|\Delta GWD_{dt,1}|$ (days to max $|\Delta GWD_{dt,1}|$) was achieved after the beginning of the dry period. Finally, we depicted the mean $|\overline{\Delta GWD_{dt,1}}|$ over time calculated for grid nodes having the same days to max $|\Delta GWD_{dt,1}|$ (lines depicted with different colours). (c) Is the same as (b) but for $z = 2$

## 4 | DISCUSSION

This study aimed to explore the use of a fully coupled surface-subsurface hydrological model for mechanistically disentangling the processes regulating stream discharge diel fluctuations in an agricultural catchment. Such model was necessary to account for the nonlinear interplays among time-varying meteorological conditions,

spatially different vegetation classes and complex topography regulating the feedbacks between soil water uses by vegetation and its flowpaths from groundwater to surface water. Given the lack of accurate input data, especially in the subsurface, and keeping in mind the primary aims of this research, we assumed homogeneous soil properties (except for the presence of the tile drains network) and atmospheric boundary conditions to allow for an efficient and reasonably realistic modelling of the observed diel fluctuations. Below we discuss how numerical modelling can support field scientists to deepen their investigation of streamflow diel fluctuations, to expand the insights to other components of the hydrological cycle as well as to better understand other implications linked to the observation of diel patterns in streamflow.

## 4.1 | The role of vegetation

We assumed uniform potential ET as a model input and we partitioned it along different rooting depths based on the vegetation classes. It was important to account for the rooting depth considering that adapted natural species can invest resources to cope with water scarcity by further developing root systems to access deeper water sources. In agriculture, there is a general interest in keeping the root system shallow to apply less nutrients and save money. However, this strategy might change because more frequent and longer dry periods are expected in the face of climate change and allowing the crop to develop a deeper root system would enhance plants resilience during droughts. Within this context, our sensitivity analysis on the rooting depth showed that the discharge and diel fluctuations were not largely affected by deeper root depths, but the volume of transpired water increased up to about 10% (as shown in Figure S5); this could only happen at the expense of water storages in parts of the catchment poorly connected to the stream.

Possible impacts of parameters and processes related to vegetation on simulation outputs emerged also when we modelled the inhibitory effect of oxygen stress on water use by vegetation. This analysis proved the necessity to understand and consider vegetation responses to environmental conditions for their relevant implications on water fluxes. For example, the cumulated ET over the simulation period achieved about $280 \times 10^3$ $m^3$ of water when accounting for oxygen stress in a catchment of 2.67 $km^2$ but it increased by about $100 \times 10^3$ $m^3$ of water without accounting for oxygen stress. These figures highlighted the crucial significance of ET for water budget calculations (Knight et al., 1981; Ryken et al., 2022; Trenberth et al., 2007).

In our study, we did not consider different crop coefficients in the calculation of actual ET, despite different vegetation transpiring different volumes of soil water as prescribed by time-varying and vegetation class-specific evapotranspiration coefficients (Pereira et al., 2015). Prescribing more realistic coefficients could lead to better predictions of discharge as well as subsurface water fluxes driven by a different water use by vegetation.

## 4.2 | The role of anthropic interventions

An interesting aspect of the studied catchment was the pervasive presence of tile drains, which we took into account by using an equivalent high-conductivity porous medium layer, similarly to Rozemeijer et al. (2010). Tile drains are typically installed to boost crop yields by avoiding excessive soil moisture in the roots. Tile drains work in two ways: they collect and carry away the infiltrating rain or irrigation water and they intercept the rising groundwater and similarly deliver such water to the stream. For this, the depth of tile drains would depend on several factors including the crop rooting depth, its tolerance to water stagnation as well as the local groundwater depth. Our modelling choice was driven by the extremely different spatial resolution necessary for an explicit representation of tile trains (diameter between 10 and 60 cm) within a DEM spatial resolution of $20 \times 20$ m necessary to run a process-based catchment-scale hydrological model in a reasonable time frame. This choice was supported by previous modelling studies validated against field data. De Schepper et al. (2015) used the model 'Hydrogeosphere' to conclude that the explicit representation of a tile drain system (10 cm diameter at 1 m depth) can be overall achieved through an equivalent porous media with increased saturated hydraulic conductivity (restricted to a 10 cm thick soil layer at 1 m depth) and prescribed zero pressure head at the nodes delineating the drainage network in the porous media. In the same settings, Thomas et al. (2016) showed that the explicit representation of tile drains predicted locally-specific groundwater table dynamics, while the scenario with the equivalent porous media resulted in homogeneous (spatially averaged) patterns. Muma et al. (2016) followed the same approach (approximately 10 cm thick soil layer at 1 m depth and prescribed zero pressure head at the nodes delineating the drainage network in the porous media) within CATHY and compared the predicted stream flow against a lumped 1-D model that account for tile drains ('DRAINMOD'). The two model outcomes were comparable; the major finding was the importance of the saturated hydraulic conductivity of the layers below the equivalent porous media. Recently, Boico et al. (2022) showed that catchment scale modelling of tile-drained agricultural landscapes is comparably affected by the conceptualisation of tile drains in the model and by unknown soil heterogeneities. In general, artificial structures are poorly represented in the hydrological cycle (Abbott et al., 2019) but they could be relevant in real scenarios. For example, Valayamkunnath et al. (2022) highlighted the importance of incorporating the tile-drain process into the operational configuration of the US National Water Model for more accurate flood forecasting and for more accurate water balance analyses in the tile-drained areas in the Midwestern US. In the particular case of diel fluctuations, tile drains not only accelerate the depletion of soil water but also allow the soil water to bypass (altering signal transmission) the vadose zone in between the hillslope and the receiving stream.

Anthropogenic influences on the hydrological cycle are also represented by irrigation practices (Jagermeyr et al., 2017). In the studied agricultural catchment, soil water depletion was very likely replenished by farmers through irrigation. While irrigation timing and quantity was unknown, as well as the water sources used for such

practices, there were clear short-living discharge peaks in the measured time series. Our estimation of irrigation quantities matching the rainfall deficit and timed in the early morning and late afternoon (i.e., before and after high air temperatures that may cause distress in the vegetation) matched well the timing of some of those peaks. Also, it was evident that irrigation sustained a higher base flow during dry periods as compared to the simulation without irrigation; however, irrigation did not affect, but only superposed to, the occurrence of streamflow diel fluctuations in this catchment. With the outlook of exploiting open monitoring data for improving the realism of catchment-scale hydrological models in human-impacted catchments (Celicourt et al., 2020), it is essential to establish cooperative frameworks between farmers and research institutions for boosting the exchange of crucial hydrological data (Della Chiesa et al., 2019).

### 4.3 | Implications of diel fluctuations

In line with many other field observations (Lundquist & Cayan, 2002), our observations showed diel fluctuations of discharge at the outlet of the catchment in the order of 10% of the daily mean flow. Our simulations in the reference run slightly overestimated this percentage. This ET-driven diel forcings not only reduce streamflow with direct consequences on water quantity downstream, but also contribute to water quality management and ecosystem functioning. The water concentration of solutes increases and decreases when discharge decreases and increases, respectively. Less obvious are direct changes in surface water physical properties when groundwater, with its own signature, daily changes its contribution to stream discharge. In the studied catchment, high-concentrations diel fluctuations of plant protection products were observed in the modelled dry periods (la Cecilia, Dax, Odermatt, et al., 2021). Diel changes in physical and biogeochemical properties of stream water commonly affect other interrelated diel cycles and processes, such as those producing diel cycles of pH and dissolved chemical species including oxygen, carbon, nitrogen and suspended particles among others (Nimick et al., 2011), thus corroborating the relevance of investigating the implications of ET-driven diel fluctuations with a multidisciplinary approach. In particular, diel interactions between surface water and groundwater occur in hyporheic zones, which are, therefore, characterized by and exposed to peculiar and alternating gradients of physical (e.g., temperature fluxes), chemical (i.e., solutes and contaminants exchanges) and biological (microorganisms transport and nutrients cycling) quantities and processes controlled by the boundary conditions (Boano et al., 2014). We showed that integrated surface-subsurface catchment-scale hydrological models have the capability to predict daily patterns, which can be expanded in scope, or coupled with other models, to enhance our predictions on multidisciplinary aspects related to aquatic ecosystems.

## 5 | CONCLUSIONS

As the likelihood of dry conditions in agricultural streams is increasing due to climate change, it is important to achieve realistic predictions of stream discharge and groundwater flow in the presence of vegetation during low flow periods for optimal water resources management at the catchment scale. During dry periods, diel fluctuations can reach up to 10% of mean discharge in small streams. Here, we used CATHY, a physics-based integrated surface-subsurface hydrological model, to simulate, explain, and map diel fluctuations in stream discharge and groundwater depth in a small tile-drained agricultural catchment in Switzerland. In our reference simulation, we replicated well the streamflow dynamics, including the timing of short-living streamflow peaks attributed to irrigation practises. In a series of hypothetical scenarios, we corroborated the predominant role of vegetation in driving the occurrence of diel streamflow and groundwater depth fluctuations, while irrigation did not affect the pattern to a large extent in this catchment. We further showed that the model could be used to explore the consequences of hydrological processes on the sources, magnitude and timing of the fluctuations in a catchment, demonstrating that, depending on the interplay among ET, the inhibitory role of oxygen stress on vegetation, the rooting depth, and topography, diel fluctuation can potentially extend from the hillslope to the riparian zone. In particular, the reference simulation but without irrigation revealed that fluctuations were largest where roots could access soil water but without being inhibited by excessive moisture. This occurred in the proximity of the riparian vegetation, close to the active stream network. The model capability to simulate dynamic spatial patterns of evapotranspiration fluxes, soil moisture and groundwater flows, enhanced our understanding of the role of these hydrological processes in our small catchment during dry periods. We conclude that CATHY, or similar ISSHMs working at sub-daily scales, can be used in other locations to drive the design of - or gain insights from - field monitoring campaigns collecting ecohydrological data.

#### ACKNOWLEDGEMENTS

The Authors acknowledge the collaboration with the environmental office of the Canton Thurgau. We thank Planimpuls AG Bauingenieure SIA for providing the drainage network. DLC was supported with funding by the Swiss Federal Office for the Environment and the Eawag Academic Transition Grant. We gratefully acknowledge the contribution of Anna Lievore, former student from the University of Padova, who ran preliminary simulations for the current study as part of her master's thesis. We thank the two anonymous Reviewers who helped us to improve the quality of the manuscript with their comments. Cloud Veneto is acknowledged for the use of computing and storage facilities.

#### CONFLICT OF INTEREST

The authors declare that they have no known competing financial interests or personal relationships that could have appeared to influence the work reported in this paper.

#### DATA AVAILABILITY STATEMENT

All input and ouput data from this study will be openly and publicly available through the Eawag repository ERIC at https://opendata.eawag.ch/group under the project folder "NAWA-Flowpath" to ensure that these data are FAIR: Findable, Accessible, Interoperable

and Reproducible. The CATHY model is freely available at https://bitbucket.org/cathy1_0/cathy/.

## ORCID

*Daniele la Cecilia* https://orcid.org/0000-0003-1898-7088
*Matteo Camporese* https://orcid.org/0000-0002-7505-798X

## REFERENCES

Abbott, B. W., Bishop, K., Zarnetske, J. P., Minaudo, C., Chapin, F. S., Krause, S., Hannah, D. M., Conner, L., Ellison, D., Godsey, S. E., Plont, S., Marçais, J., Kolbe, T., Huebner, A., Frei, R. J., Hampton, T., Gu, S., Buhman, M., Sayedi, S. S., … Pinay, G. (2019). Human domination of the global water cycle absent from depictions and perceptions. *Nature Geoscience*, *12*(7), 533–540. https://doi.org/10.1038/s41561-019-0374-y

Allen, R. G., Pereira, L. S., Raes, D., & Smith, M. (2006). FAO irrigation and drainage Paper No. 56. Crop evapotranspiration (guidelines for computing crop water requirements), 1–333.

Biggs, J., von Fumetti, S., & Kelly-Quinn, M. (2016). The importance of small waterbodies for biodiversity and ecosystem services: Implications for policy makers. *Hydrobiologia*, *793*(1), 3–39. https://doi.org/10.1007/s10750-016-3007-0

Boano, F. J., Harvey, W., Marion, A., Packman, A. I., Revelli, R., Ridolfi, L., & Wörman, A. (2014). Hyporheic flow and transport processes: Mechanisms, models, and biogeochemical implications. *Reviews of Geophysics*, *52*, 603–679.

Boico, V. F., Therrien, R., Delottier, H., Young, N. L., & Højberg, A. L. (2022). Comparing alternative conceptual models for tile drains and soil heterogeneity for the simulation of tile drainage in agricultural catchments. *Journal of Hydrology*, *612*, 128120. https://doi.org/10.1016/j.jhydrol.2022.128120

Bond, B. J., Jones, J. A., Moore, G., Phillips, N., Post, D., & McDonnell, J. J. (2002). The zone of vegetation influence on baseflow revealed by diel patterns of streamflow and vegetation water use in a headwater basin. *Hydrological Processes*, *16*, 1671–1677.

Bosch, J. M., & Hewlett, J. D. (1982). A review of catchment experiments to determine the effect of vegetation changes on water yield and evapotranspiration. *Journal of Hydrology*, *55*, 3–23.

Bradford, M. J., & Heinonen, J. S. (2008). Low flows, instream flow needs and fish ecology in small streams. *Canadian Water Resources Journal*, *33*(2), 165–180. https://doi.org/10.4296/cwrj3302165

Bren, L. (1997). Effects of slope vegetation removal on the diurnal variations of a small mountain stream. *Water Resources Research*, *33*, 321–331.

Brunner, P., Therrien, R., Renard, P., Simmons, C. T., & Franssen, H.-J. H. (2017). Advances in understanding river-groundwater interactions. *Reviews of Geophysics*, *55*(3), 818–854. https://doi.org/10.1002/2017rg000556

Burt, T. P. (1979). Diurnal variations in stream discharge and throughflow during a period of low flow. *Journal of Hydrology*, *41*, 291–301.

Camporese, M., Daly, E., & Paniconi, C. (2015). Catchment-scale Richardsequation-based modeling ofevapotranspiration via boundary-condition switching and root wateruptake schemes. *Water Resources Research*, *51*, 5756–5771.

Camporese, M., Paniconi, C., Putti, M., & Orlandini, S. (2010). Surface-subsurface flow modeling with path-based runoff routing, boundary condition-based coupling, and assimilation of multisource observation data. *Water Resources Research*, *46*, W02512.

Carsel, R. F., & Parrish, R. S. (1988). Developing joint probability distributions of soil water retention. *Water Resources Research*, *24*, 755–769.

Celicourt, P., Rousseau, A. N., Gumiere, S. J., & Camporese, M. (2020). Agricultural hydroinformatics: A blueprint for an emerging framework to Foster water management-centric sustainability transitions in farming systems. *Frontiers in Water*, *2*, 586516. https://doi.org/10.3389/frwa.2020.586516

Constantz, J. (1998). Interaction between stream temperature, streamflow, and groundwater exchanges in alpine streams. *Water Resources Research*, *34*, 1609–1615.

Czikowsky, M., & Fitzjarrald, D. (2004). Evidence of seasonal changes in evapotranspiration in eastern US hydrological records. *Journal of Hydrometeorology*, *5*, 974–988.

Della Chiesa, S., la Cecilia, D., Genova, G., Balotti, A., Thalheimer, M., Tappeiner, U., & Niedrist, G. (2019). Farmers as data sources: Cooperative framework for mapping soil properties for permanent crops in South Tyrol (Northern Italy). *Geoderma*, *342*, 93–105. https://doi.org/10.1016/j.geoderma.2019.02.010

De Schepper, G., Therrien, R., Refsgaard, J. C., & Hansen, A. L. (2015). Simulating coupled surface and subsurface water flow in a tile-drained agricultural catchment. *Journal of Hydrology*, *521*, 374–388. https://doi.org/10.1016/j.jhydrol.2014.12.035

Floriancic, M. G., Berghuijs, W. R., Molnar, P., & Kirchner, J. W. (2021). Seasonality and drivers of low flows across Europe and the United States. *Water Resources Research*, *57*(9), e2019WR026928. https://doi.org/10.1029/2019wr026928

Gupta, H. V., Kling, H., Yilmaz, K. K., & Martinez, G. F. (2009). Decomposition of the mean squared error and NSE performance criteria: Implications for improving hydrological modelling. *Journal of Hydrology*, *377*(1–2), 80–91. https://doi.org/10.1016/j.jhydrol.2009.08.003

Gutmann, F., & Simmons, L. M. (1952). The temperature dependence of the viscosity of liquids. *Journal of Applied Physics*, *23*, 977–978.

Harmon, R., Barnard, H. R., & Singha, K. (2020). Water table depth and bedrock permeability control magnitude and timing of transpiration-induced diel fluctuations in groundwater. *Water Resources Research*, *56*(5), e2019WR025967. https://doi.org/10.1029/2019wr025967

Haslinger, K., Koffler, D., Schöner, W., & Laaha, G. (2014). Exploring the link between meteorological drought and streamflow: Effects of climate-catchment interaction. *Water Resources Research*, *50*(3), 2468–2487. https://doi.org/10.1002/2013wr015051

Jagermeyr, J., Pastor, A., Biemans, H., & Gerten, D. (2017). Reconciling irrigated food production with environmental flows for sustainable development goals implementation. *Nature Communications*, *8*, 15900. https://doi.org/10.1038/ncomms15900

Kirchner, J. W., Godsey, S. E., Solomon, M., Osterhuber, R., McConnell, J. R., & Penna, D. (2020). The pulse of a montane ecosystem: Coupling between daily cycles in solar flux, snowmelt, transpiration, groundwater, and streamflow at Sagehen Creek and Independence Creek, Sierra Nevada, USA. *Hydrology and Earth System Sciences*, *24*(11), 5095–5123. https://doi.org/10.5194/hess-24-5095-2020

Knight, D., Fahey, T., & Running, S. (1981). Whole-tree potometers estimate pine forest transpiration. *Bioscience*, *31*, 242–243.

la Cecilia, D., Dax, A., Ehmann, H., Koster, M., Singer, H., & Stamm, C. (2021). Continuous high-frequency pesticide monitoring to observe the unexpected and the overlooked. *Water Research X*, *13*, 100125. https://doi.org/10.1016/j.wroa.2021.100125

la Cecilia, D., Dax, A., Odermatt, D., Singer, H., & Stamm, C. (2021). High-concentrations diel-fluctuations of plants protection products in dry periods. EGU General Assembly 2021, 1. https://doi.org/10.5194/egusphere-egu21-14188

Lawrence, R. E. (1990). The interaction between the environment, land use, and hydrology of the Bogong High Plains area from 1850 to 1985. [Doctoral dissertation, The University of Melbourne].

Lundquist, J. D., & Cayan, D. R. (2002). Seasonal and spatial patterns in diurnal cycles in streamflow in the Western United States. *Journal of Hydrometeorology*, *3*, 591–603.

Mastrotheodoros, T., Pappas, C., Molnar, P., Burlando, P., Manoli, G., Parajka, J., Rigon, R., Szeles, B., Bottazzi, M., Hadjidoukas, P., & Fatichi, S. (2020). More green and less blue water in the Alps during

warmer summers. *Nature Climate Change*, *10*(2), 155–161. https://doi.org/10.1038/s41558-019-0676-5

Muma, M., Rousseau, A. N., & Gumiere, S. J. (2016). Modeling of subsurface agricultural drainage using two hydrological models with different conceptual approaches as well as dimensions and spatial scales. *Canadian Water Resources Journal/Revue canadienne des ressources hydriques*, *42*(1), 38–53. https://doi.org/10.1080/07011784.2016.1231014

Nash, J. E., & Sutcliffe, J. V. (1970). River flow forecasting through conceptual models part I: A discussion of principles. *Journal of Hydrology*, *10*, 282–290.

Nimick, D. A., Gammons, C. H., & Parker, S. R. (2011). Diel biogeochemical processes and their effect on the aqueous chemistry of streams: A review. *Chemical Geology*, *283*(1–2), 3–17. https://doi.org/10.1016/j.chemgeo.2010.08.017

O'Laughlin, E. M., Cheney, N. P., & Burns, J. (1982). The bushrangers experiment: Hydrological response of a eucalypt catchment to fire. In E. M. O'Laughlin & L. J. Bren (Eds.), *The first National Symposium on Forest hydrology* (pp. 132–139). Institute of Engineering of Australia.

Paniconi, C., & Putti, M. (2015). Physically based modeling in catchment hydrology at 50: Survey and outlook. *Water Resources Research*, *51*(9), 7090–7129. https://doi.org/10.1002/2015wr017780

Pereira, L. S., Allen, R. G., Smith, M., & Raes, D. (2015). Crop evapotranspiration estimation with FAO56: Past and future. *Agricultural Water Management*, *147*, 4–20. https://doi.org/10.1016/j.agwat.2014.07.031

Roderick, M. L., Sun, F., Lim, W. H., & Farquhar, G. D. (2014). A general framework for understanding the response of the water cycle to global warming over land and ocean. *Hydrology and Earth System Sciences*, *18*(5), 1575–1589. https://doi.org/10.5194/hess-18-1575-2014

Rozemeijer, J. C., van der Velde, Y., McLaren, R. G., van Geer, F. C., Broers, H. P., & Bierkens, M. F. P. (2010). Integrated modeling of groundwater-surface water interactions in a tile-drained agricultural field: The importance of directly measured flow route contributions. *Water Resources Research*, *46*(11), W11537. https://doi.org/10.1029/2010wr009155

Ryken, A. C., Gochis, D., & Maxwell, R. M. (2022). Unravelling groundwater contributions to evapotranspiration and constraining water fluxes in a high-elevation catchment. *Hydrological Processes*, *36*(1), e14449. https://doi.org/10.1002/hyp.14449

Schwab, M., Klaus, J., Pfister, L., & Weiler, M. (2016). Diel discharge cycles explained through viscosity fluctuations in riparian inflow. *Water Resources Research*, *52*(11), 8744–8755. https://doi.org/10.1002/2016wr018626

Smakhtin, V. U. (2001). Low flow hydrology: A review. *Journal of Hydrology*, *240*, 147–186.

Szeles, B., Broer, M., Parajka, J., Hogan, P., Eder, A., Strauss, P., & Bloschl, G. (2018). Separation of scales in transpiration effects on low flows: A spatial analysis in the hydrological open air laboratory. *Water Resources Research*, *54*(9), 6168–6188. https://doi.org/10.1029/2017WR022037

Teuling, A. J., Van Loon, A. F., Seneviratne, S. I., Lehner, I., Aubinet, M., Heinesch, B., Bernhofer, C., Grünwald, T., Prasse, H., & Spank, U. (2013). Evapotranspiration amplifies European summer drought. *Geophysical Research Letters*, *40*(10), 2071–2075. https://doi.org/10.1002/grl.50495

Thomas, N. W., Arenas, A. A., Schilling, K. E., & Weber, L. J. (2016). Numerical investigation of the spatial scale and time dependency of tile drainage contribution to stream flow. *Journal of Hydrology*, *538*, 651–666. https://doi.org/10.1016/j.jhydrol.2016.04.055

Trenberth, K. E., Smith, L., Qian, T., Dai, A., & Fasullo, J. (2007). Estimates of the global water budget and its annual cycle using observational and model data. *Journal of Hydrometeorology*, *8*, 758–769.

Turk, L. J. (1975). Diurnal fluctuations of water tables induced by atmospheric–pressure changes. *Journal of Hydrology*, *26*, 1–16.

Van Genuchten, M. T. (1980). A closed form equation for predicting the hydraulic conductivity of unsaturated soils. *Soil Science Society of America Journal*, *44*, 892–898. https://doi.org/10.2136/sssaj1980.03615995004400050002x

Valayamkunnath, P., Gochis, D. J., Chen, F., Barlage, M., & Franz, K. J. (2022). Modeling the hydrologic influence of subsurface tile drainage using the National Water Model. *Water Resources Research*, *58*(4), e2021WR031242. https://doi.org/10.1029/2021wr031242

Willmott, C. J. (1984). On the evaluation of model performance IN physical geography. *Spatial Statistics and Models*, *40*, 443–460.

Wohl, E. (2017). The significance of small streams. *Frontiers of Earth Science*, *11*(3), 447–456. https://doi.org/10.1007/s11707-017-0647-y

## SUPPORTING INFORMATION

Additional supporting information can be found online in the Supporting Information section at the end of this article.

**How to cite this article:** la Cecilia, D., & Camporese, M. (2022). Resolving streamflow diel fluctuations in a small agricultural catchment with an integrated surface-subsurface hydrological model. *Hydrological Processes*, *36*(12), e14768. https://doi.org/10.1002/hyp.14768